Carbohydrate Polymers

Effect of thermal treatments on chiral nematic cellulose nanocrystal films

--Manuscript Draft--

Manuscript Number:	CARBPOL-D-21-01689R1
Article Type:	Research Paper
Keywords:	Cellulose Nanocrystals; cross-linking; carbonisation; chiral carbon; Thermal stability; photonic pigments
Corresponding Author:	Silvia Vignolini Cambridge Cambridge, UNITED KINGDOM
First Author:	Giulia Guidetti, Ph.D
Order of Authors:	Giulia Guidetti, Ph.D
	Bruno Frka-Petesic, Ph.D
	Ahu G. Dumanli, Ph.D
	Wadood Y. Hamad, Ph.D
	Silvia Vignolini, Ph.D
Abstract:	The ability to manipulate the optical appearance of materials is essential in virtually all products and areas of technology. Structurally coloured chiral nematic cellulose nanocrystal (CNC) films proved to be an excellent platform to design optical appearance, as their response can be moulded by organising them in hierarchical architectures. Here, we study how thermal treatments influence the optical appearance of structurally coloured CNC films. We demonstrate that the CNCs helicoidal architecture and the chiral optical response can be maintained up to 250°C, while the helicoidal arrangement can be further preserved up to 900°C, thus producing aromatic chiral carbon. The ability to retain the helicoidal arrangement, and thus the visual appearance, in CNC films up to 250°C is highly desirable for high temperature colour-based industrial applications and for passive colorimetric heat sensors. Similarly, the production of chiral carbon provides a new type of conductive carbon for electrochemical applications.

Effect of thermal treatments on chiral nematic cellulose nanocrystal films

Giulia Guidetti[a,b], *Bruno Frka-Petesic*[a], *Ahu G. Dumanli*[a,c,d], *Wadood Y. Hamad*[e] *and Silvia Vignolini*[a,*]

[a] Melville laboratory for Polymer synthesis, Department of Chemistry, University of Cambridge, Lensfield Road, CB2 1EW, United Kingdom

[b] Current address: Silklab, Department of Biomedical Engineering, Tufts University, 200 Boston Avenue, Medford, MA 02155, USA

[c] Current address: Department of Materials, Oxford Road, The University of Manchester, Manchester, M13 9PL, UK

[d] Current address: Henry Royce Institute, Oxford Road, The University of Manchester, Manchester, M13 9PL, UK

[e] Bioproducts Innovation Centre of Excellence, FPInnovations, 2665 East Mall, Vancouver, BC, Canada V6T 1Z4

* Corresponding author. E-mail: sv319@cam.ac.uk; Phone: +44-1223-761490

Email Addresses

GG: giulia.guidetti@tufts.edu

BFP: bf284@cam.ac.uk

AGD: ahugumrah.parry@manchester.ac.uk

WYH: wadood.hamad@fpinnovations.ca

SV: sv319@cam.ac.uk

Abstract

The ability to manipulate the optical appearance of materials is essential in virtually all products and areas of technology. Structurally coloured chiral nematic cellulose nanocrystal (CNC) films proved to be an excellent platform to design optical appearance, as their response can be moulded by organising them in hierarchical architectures. Here, we study how thermal treatments influence the optical appearance of structurally coloured CNC films. We demonstrate that the CNCs helicoidal architecture and the chiral optical response can be maintained up to 250 °C, while the helicoidal arrangement can be further preserved up to 900 °C, thus producing aromatic chiral carbon. The ability to retain the helicoidal arrangement, and thus the visual appearance, in CNC films up to 250 °C is highly desirable for high temperature colour-based industrial applications and for passive colorimetric heat sensors. Similarly, the production of chiral carbon provides a new type of conductive carbon for electrochemical applications.

Keywords

Cellulose nanocrystals, cross-linking, carbonisation, chiral carbon, thermal stability, photonic pigments

1. Introduction

Cellulose nanocrystals (CNCs), as extracted from wood pulp and cotton and dispersed in an aqueous phase, can spontaneously form a chiral nematic liquid crystalline phase that can be retained in solid state films (J.-F. F. Revol et al., 1992, 1998). The helicoidal arrangement of birefringent rod-like CNCs causes the reflection of circularly polarised light in the specular direction (Dumanli et al., 2014; Frka-Petesic et al., 2015; Marchessault et al., 1959). While the

reflected or diffracted colour can be tuned by controlling the cellulose nanocrystal suspension properties (Beck-Candanedo et al., 2005; Dong et al., 1998; Elazzouzi-Hafraoui et al., 2008; J.-F. Revol et al., 1997) or the drying history (Beck et al., 2013; Frka-Petesic et al., 2019; Zhao et al., 2019), the directionality of the reflection (Frka-Petesic et al., 2019) can, instead, be tuned exploiting external forces (Cao et al., 2020; Frka-Petesic, Guidetti, et al., 2017; Frka-Petesic, Radavidson, et al., 2017) or confinement of the drying suspension (Parker et al., 2016, 2018). For such unique properties, CNC films are a particularly interesting system for the production of renewable photonic pigments that can find application in anti-counterfeiting devices, in the textiles, food and cosmetic industries. The heat treatment of CNC films can be both detrimental, as it degrades the films' optical properties, but can also be advantageous, as it can allow the development of *e.g.*, chiral carbonaceous electrodes. In particular, industrial processes often require the use of melt-extrusion processes for the fabrication of composite materials; therefore, to use chiral nematic CNC films as photonic pigments it is necessary to tune their thermal resistance to prevent the loss of structural integrity and of the coloration due to the cellulose degradation at high temperatures. On the other hand, high temperature treatments (*e.g.*, carbonisation) that lead to the controlled decomposition of CNC films into chiral carbonaceous structures can be interesting for the development of conductive chiral nanostructured substrates for electrochemical applications.

The thermal stability of chiral nematic CNC films refers to structural, chemical, and optical integrity of the films at high temperatures as the helicoidal arrangement, the cellulose nanorods composition, and their birefringence are all necessary properties to obtain the chiral optical response. Therefore, the CNCs source and extraction protocols are important parameters to take into account when performing thermal treatments. Structural stability of the CNCs at high temperatures is usually increased by using highly crystalline sources, such as wood pulp rather than cotton. Moreover, during the acid hydrolysis of cellulose, employed to obtain CNCs that

75 self-assemble into films with helicoidal nanoarchitecture, some hydroxyl groups at the surface
76 of the crystalline domains are esterified to give negatively charged sulfate half-ester groups (–
77 OSO_3^-) (Hamad & Hu, 2010; Marchessault et al., 1959). These surface charges are one of the
78 driving forces for the CNCs to self-assemble into a chiral nematic phase; at the same time, this
79 charge substitution extends only to the primary hydroxyl groups while the secondary hydroxyl
80 groups are unaffected (Dong et al., 1998). The sulfate half-ester groups and the remaining
81 secondary hydroxyl groups on the CNCs surface are reactive centres that can, therefore,
82 promote an earlier thermal degradation unless stabilised by further functionalisation or by
83 cross-linking (Beck & Bouchard, 2014; Eyley & Thielemans, 2014; Lin & Dufresne, 2014;
84 Roman & Winter, 2004; Wang et al., 2007). Specifically, the presence of the $–OSO_3^-$ groups
85 can cause hydrolysis and release sulfuric acid, leading to the chiral nematic CNC films
86 degradation for temperatures as low as 150 °C. Consequently, the choice of polymers for the
87 fabrication of structurally coloured CNC-based composites, *via* hot-melt extrusion processes,
88 has been so far limited to polar polymers with a lower melting point.

89 Efforts on increasing CNCs structural and chemical stability at high temperatures have
90 suggested the use of weaker acids (Camarero Espinosa et al., 2013) or ionic liquids (Lazko et
91 al., 2014) for the hydrolysis step, and the decrease of the concentration (Beck & Bouchard,
92 2014) or pH neutralization (Acierno et al., 2020; Nan et al., 2017) of the sulfate half-ester
93 groups on the CNCs surface. Most of these techniques are, however, applied on the CNCs
94 when in the liquid phase, thus changing their ionic interactions and prohibiting the transition
95 to a chiral nematic phase that can lead to chiral nematic solid films upon drying. In contrast,
96 approaches such as cross-linking offer a significant advantage to improve the thermostability
97 of polymeric materials (Hennink & van Nostrum, 2012; Mane et al., 2016) as it is possible to
98 apply the cross-linker directly on solid CNC films, therefore, allowing for greater variability
99 of optical properties. Specifically, CNCs allow for a variety of chemical cross-linking types

due to their high surface area and their tuneable surface charges. For instance, bacterial cellulose has been reported to be successfully cross-linked by glutaraldehyde, (GA) (Brown et al., 2012), which can cross-link hydroxyl and amine groups and thus it has been commonly used for deacetylated chitin, chitosan and cellulose (Chan et al., 2019; Dai & Barbari, 1999; Hennink & van Nostrum, 2012; Wine et al., 2007).

Here, we investigate the effect of thermal treatments on the optical response of structurally coloured CNC films, promoting cellulose decomposition directly into carbon. We demonstrate that our methodology allows for the fabrication of CNC films that retain the helicoidal architecture, while also homogeneously improving the colour contrast, resulting in films with minimal thermal darkening, which can be used for industrial processes with working temperatures as high as 250 °C and as passive colorimetric sensors of past heat exposure. In particular, we first show that a good colouration in thin films can be retained for temperatures up to 250 °C by first immersing the films in a concentrated base (KOH), then cross-linking with glutaraldehyde and, finally, performing a thermal treatment under inert atmosphere at 250 °C (hypothesis 1). Then, we show a second methodology to preserve the helicoidal architecture of CNC films up to 900 °C, therefore generating chiral carbon, without the need for hard templating (hypothesis 2). The evolution of the helicoidal architecture of CNC films at different thermal treatment temperatures (T_{room}, 250 °C, and 900 °C) is monitored using polarised optical microscopy, while their structural integrity is investigated by scanning electron microscopy (SEM). The pre-treatments effect on the chemical stability is evaluated by thermogravimetric analysis (TGA), while the structural transformations induced by the thermal treatments are monitored via Fourier-transform infrared (FTIR) spectroscopy.

2. Material and methods

2.1 Materials

Sodium hydroxide, potassium hydroxide and glutaraldehyde were purchased from Sigma Aldrich. All chemicals were used as received. The wood pulp suspension of cellulose nanocrystals (CNCs) was provided by CelluForce Inc., at pH 2.2 and with [-OSO_3^-] = 243 mmol/kg, as measured by titration against NaOH, and stored at 4 °C when not in use.

2.2 Cellulose nanocrystal films preparation

The cellulose nanocrystal films were prepared by evaporation-induced-self-assembly (EISA). The CNC suspension was vortexed for about 1 minute to ensure homogeneity before casting (Gallenkamp, Spinmix, 50–60 Hz, 220-240 Volts, 90 Watts) and poured on non-treated polystyrene Petri dishes (35 mm internal diameter, 10 mm height Corning®, 430588). The suspension was allowed to dry at ambient conditions in a drying cabinet containing silica gel beads (Acros, 2–5 mm, 1327-36-2). The drying time varied from 3 to 7 days depending on the suspension volume and concentration. The dry films were detached from the substrate and stored in a dry cabinet until further use. The films used for the KOH treatment and cross-linking were cast from 3 mL of 2 wt% suspension, whereas those used for the vacuum treatment were cast from 1 mL of 2 wt% suspension.

The CNC dry films were pH-neutralised by immersing them in 30 wt% potassium hydroxide (KOH) solution in water for 24 hours at room temperature. The films were then gently rinsed with warm MQ water (T ∽ 50 °C), until the pH of the rinsing water was stable and equal to 7. This rinsing step allowed for the removal of the remaining KOH. The samples were left to dry in a drying box at room temperature until further use. The sample curling upon drying was minimised by a rigid sheet of polytetrafluoroethylene placed on top of the CNC films.

CNC films cross-linked with glutaraldehyde (GA) were fabricated starting from free-standing CNC films that were infiltrated in KOH for 24 h following the above-described protocol and subsequently immersed in 8 mL 25 wt% GA at 70 °C for 5 h. The films were successively retrieved from the GA solution, dried in an air oven at 70 °C for 1 h and dried in a vacuum oven at 60 °C overnight to ensure effective water removal.

CNC films used for vacuum treatment were cast from a suspension heat treated in a water bath at 60 °C for 24 h. Once dry, the films were peeled off from the polystyrene Petri dish and desiccated in a vacuum oven at 60 °C for 5 days. All the samples were stored in a drying box until further use.

2.3 Thermal treatment

Cellulose nanocrystal films were heat treated in a Carbolite Gero split tube furnace. Free-standing films were positioned in an alumina boat and kept flat by using quartz slides on the edges of the films to prevent curling. A perforated quartz slide was positioned on top of the alumina boat to prevent the flakes from being blown away by the gas flow. The ceramic boat containing the flakes was placed inside a quartz cylinder (l = 65 mm, $Ø_{int}$ = 29 mm, $Ø_{out}$ = 32 mm) in the central part of the furnace to provide homogeneous heating. To ensure complete sealing of the quartz tube, it was connected to the gas hoses with metallic end seals (TS-032-042-0020, Carbolite Gero) and greased. For optimal thermal insulation, ceramic insulating plugs were inserted at both ends of the quartz tube (51-50-11, type D, Carbolite Gero). The thermal treatments were carried out under continuous Argon flow. The gas flow was controlled with a flow-meter set at 200 mL/min and the exhaust gas was directed in an oil bubbler to prevent reflux in the furnace. The heating ramps followed during the heat treatment were the following: for the heat treatments up to 250 °C we used 1°C/min, while for the heat treatments

up to 900 °C we used 1 °C/min from room temperature up to 300 °C, then 3 °C/min from 300 °C to 500 °C, and finally 5 °C/min from 500 °C to 900 °C. Before each heat treatment, the samples were inserted in the furnace, which was then tightly sealed, and stabilised at room temperature under 200 mL/min argon flow for 1 h, to ensure complete removal of air by replacement with argon gas. After the heating ramp, the samples were left to naturally cool down inside the furnace under continuous argon flow at 200 mL/min until room temperature.

2.4 Polarised optical microscopy

The films were analysed in bright field reflection on a customised Zeiss Axio Microscope using a Halogen lamp (Zeiss HAL100) as a light source with Koehler illumination. The light reflected off the samples passed through a quarter wave plate and a polarizing filter, specifically oriented to let only left-circularly polarized or right-circularly polarized light pass before being split between a CCD camera (Thorlabs DCC3240C) and an optical fibre mounted in confocal configuration and connected to a spectrometer (AvaSpec-HS2048, Avantes). This set-up allows for the spectral acquisition from specific areas in the samples; all the spectra were normalized to the reflection of a silver mirror in one polarization channel. Macroscopic pictures of the analysed films were taken using a Canon DSLR camera.

2.5 Scanning electron microscopy

The morphological properties of the CNC films were studied using a Leo Gemini 1530VP, Zeiss, scanning electron microscope, operating in high vacuum mode at 5 kV accelerating voltage and working distance 3–4 mm with an Inlens secondary electron detector. To study the internal structure of the CNC films, samples were mounted on aluminium stubs at an angle of 90° with respect to the electron beam, exposing the cross-section. To minimise charging effects the films were fixed on the stub using conductive carbon tape and were subsequently sputter-

196 coated with a 5-10 nm thick layer of Au/Pd to minimise the charging effect (Emitech K550; I
197 = 55 mA for 10–14 s).
198
199 *2.6 Thermogravimetric analysis*
200 The decomposition behaviour of the fabricated CNC films was studied in a thermo gravimetric
201 analyser (TGA 2 (SF), Mettler Toledo). CNC film flakes (~10 mg) were put in an Al_2O_3
202 crucible, which was positioned on a balance arm and heated from 50 °C to 900 °C with a heating
203 rate of 10 °C/min in continuous nitrogen flow at 100 mL/min. The first derivative of the mass
204 change as a function of the time was calculated and defined as derivative-TGA (DTGA). The
205 software *Matlab R2016B* and *STARe Evaluation Software* were used to calculate the maximum
206 degradation peak, T_{max}, the onset temperature, T_{onset}, the temperature for which 10% and then
207 half of the material has degraded, T_{10} and T_{50}, and the yield, Y. The onset degradation
208 temperature was defined as the intersection of tangents drawn from thermogravimetric curves,
209 one before inflection caused by the degradation and another from the cellulose degradation
210 step.
211
212 *2.7 Fourier Transformed Infrared Spectroscopy*
213 The transmittance spectra were measured using a Bruker Alpha II spectrometer in the range
214 4000-400 cm^{-1} with a resolution of 2 cm^{-1} and 64 averages.
215
216 *2.8 X-ray Crystallographic Analysis*
217 The X-ray diffractograms of the CNC films were acquired using a PANalytical X-ray
218 diffractometer operating with a Cu Kα radiation source (λ = 1.5405 Å) generated at 40 kV and
219 40 mA and recorded in the 2θ range of 5º-40º using 0.017º increments for 25 minutes at room
220 temperature.

221

222 *3. Results and Discussion*

223 We fabricated a series of different CNC films for the investigation of the morphological,
224 optical, and structural changes upon thermal treatment, as presented in Table S1. All the films
225 were cast from acidic CNC suspensions (*i.e.*, with H^+ as counter-ions) and treated as reported
226 in the Experimental Section. The fabricated films were: 1) as-cast CNC films used as an acidic
227 control (CNC-A); 2) CNC-A films further processed by immersion in a potassium hydroxide
228 bath for 24 h followed by extensive rinsing with milli-Q water, used as a pH-neutral control
229 (CNC-A-N); 3) CNC-A-N films further immersed in glutaraldehyde (GA), cross-linked and
230 dried (CNC-A-N-GA); 4) CNC-A films exposed to vacuum for five days (CNC-A-Vac). These
231 CNC films were then heat treated under inert atmosphere either at 250 °C (CNC-A-N-250 and
232 CNC-A-N-GA-250) or at 900 °C (CNC-A-N-GA-900 and CNC-A-Vac-900).

233 Notably, similarly to NaOH, treating CNC films with KOH can induce the mercerisation of the
234 cellulose and the transformation of the crystalline structure from Cellulose I to Cellulose II
235 (Figure S1). This polymorphic transformation is characterized by the irreversible shift of the
236 crystalline peaks generated by the family of planes {100} and {200} from 2Θ = 14-17º to 12º
237 and from 2Θ=23º to 20-21º, respectively (Nan et al., 2017; J. Revol & Goring, 1981). The
238 cross-linking reaction between CNCs and glutaraldehyde consists in the formation of acetal
239 bridges between the residual hydroxyl group of the CNCs and the aldehyde under alkaline
240 conditions (Brown et al., 2012; Hennink & van Nostrum, 2012; Wine et al., 2007), which are
241 also known to favour the glutaraldehyde polymerization leading to the formation of poly-
242 glutaraldehyde (Migneault et al., 2004).

243 The investigated thermal treatments temperatures were set at T=250 °C and T=900 °C. At
244 T=250 °C the cellulose in KOH-treated CNC films did not appear to have optically degraded
245 much yet; therefore, we chose this temperature to ensure the non-degradation of the CNCs

chiral optical response while also being a temperature that is high enough to be compatible with thermoplastic materials and melt-extrusion industrial processes. In contrast, T=900 °C was chosen to have a full decomposition of the CNCs into aromatic carbon, therefore allowing for good electrical conductivity (Dumanli & Windle, 2012).

The microscopic chiral optical response of CNC-A-N films with and without the cross-linking agent was investigated by macroscopic photography (Figure S2) and by polarized optical microscopy (Figure 1).

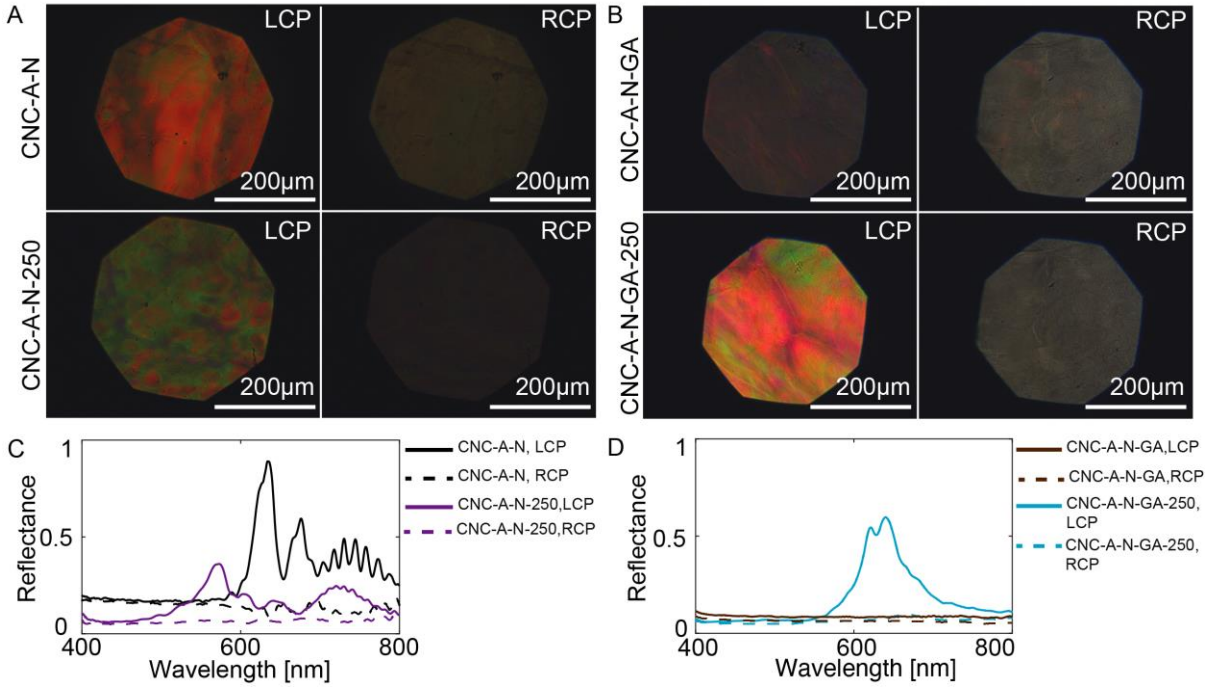

Figure 1. Optical analysis of the cross-linking effect on CNC films at room temperature and after thermal treatment at 250 °C. (**A**, **B**) Polarised optical microscopy images and (**C**, **D**) corresponding reflectance spectra, normalised to a silver mirror in one polarisation channel of (**A**, **C**) CNC-A-N films and (**B**, **D**) CNC-A-N-GA films at room temperature and after thermal treatment at 250 °C. The bright field reflectance micrographs and the corresponding spectra are shown both for the left- and for the right-circular polarisation channel, respectively, LCP and RCP.

Before the thermal treatments (T_{room}) both the CNC-A-N film and the CNC-A-N-GA film display polarisation-selective reflection: they reflect left-circularly polarised (LCP) light and transmit right-circularly polarised (RCP) light, as shown by the micrographs of Figure 1, A and B, and by the corresponding reflectance spectra reported in Figure 1, C and D. Only minimal

coloration is observed for the RCP reflection both for the CNC-A-N and the CNC-A-N-GA films, thus indicating the presence of helicoidal domains with uniform orientation in the films (Frka-Petesic, Guidetti, et al., 2017; Parker et al., 2018). Since the CNC-A-N film reflects red light, after the infiltration with the GA, the reflectance is red-shifted to near IR and no difference between the LCP and RCP can be measured in the visible range. The presence of an internal helicoidal arrangement in the CNC-A-N-GA films and in the CNC-A-N films is also confirmed by scanning electron microscopy (SEM), as illustrated by the film cross-sections shown in Figure 2, A and B (T_{room}). The cross-linking of the CNC films induces the formation of a compact pseudo-layer structure with long-range order and helicoidal architecture, Figure 2B. Macroscopically, after the heat treatment at 250 °C, CNC-A-N films show minimal scattering, but also little coloration due to the excessive darkening, which has been ascribed to cellulose dehydration during the thermal treatment (Dumanli & Windle, 2012; Vignolini et al., 2016) (Figure S2). These films appear darker both on white and on black backgrounds, especially at the edge, possibly due to a higher local concentration of sulfuric acid at the edge of the film arising from the drying front that starts from the centre to the edge of the dish. As this darkening was observed both in thin and thick films, we speculate to be independent from the thickness (that can also vary at the edge); rather, we believe it could be caused by the gradient of free sulfuric acid released during the heat treatment from the CNCs surface (Beck & Bouchard, 2014). This excessive darkening can easily overpower the structural colour of the CNC films. However, this darkening can also be reduced in presence of a cross-linker in the CNC films, such as the glutaraldehyde (GA), as shown in Figure S2 (Beck & Bouchard, 2014). Macroscopically, in the thermally treated cross-linked films, strong blackening is only observed at the very edge of the films, where the helicoidal arrangement of the CNCs is less pronounced. The larger portion of the films displays the structural colour typical of chiral nematic CNC films with minimal darkening.

Microscopically, the optical response of the films after heat treatment at 250 °C shows a clear chiral response in the visible range, supported both by the micrographs with bright colours and by the broad reflection peaks visible only in LCP in Figure 1. The blue-shift in the reflected light is expected from the thermally-induced shrinking and confirms that the helicoidal arrangement can be retained in both CNC-A-N and in CNC-A-N-GA films after a heat treatment at 250 °C; the chiral nematic nature of the films is also confirmed by the SEM cross-sections showing a tightly packed helicoidal arrangement (Figure 2C, D).

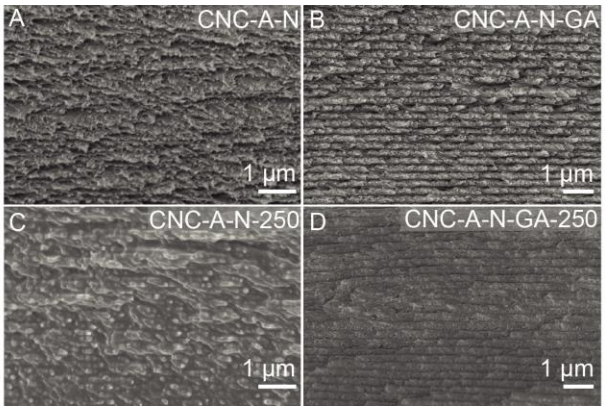

Figure 2. SEM of CNC films cross-sections before and after crosslinking with GA, at room temperature and after thermal treatment at 250 °C. The typical periodic structure indicative of the helicoidal architecture is visible for the CNC-A-N films both before (**A**) and after (**C**) the thermal treatment at 250 °C. Similarly, in cross-linked films the periodic structure observed at room temperature (CNC-A-N-GA) (**B**) is retained after the thermal treatment (CNC-A-N-GA-250) (**D**).

To investigate the CNC-A-N and CNC-A-N-GA films evolution with the thermal treatment, Fourier-transform infrared spectroscopy (FTIR) was conducted, as reported in Figure 3. Before the thermal treatment, the typical transmission peaks of cellulose can be seen for the CNC-A-N film and for CNC-A-N-GA films, which are: single bond O-H (3300 cm^{-1}), C-H (2900 cm^{-1}), C-O (1022 cm^{-1}), and C-O-H (1160 cm^{-1}) stretching, C-H (1431 cm^{-1}) deformation stretching and CH_2 (1427 cm^{-1}) bending (Guidetti et al., 2016). Moreover, for the CNC-A-N-GA film the additional double bond C=O stretching typical of GA is visible at 1720 cm^{-1}. After the thermal treatment, the cellulose dehydration induces the formation of double bonds C=O, whose stretching signal can be seen at 1720 cm^{-1} both for thermally treated CNC-A-N films

and for the CNC-A-N-GA films (Ţucureanu et al., 2016). Therefore, at 250 °C most of the typical cellulose FTIR signals are retained as expected due to the early stage of the cellulose decomposition that occurs for such low thermal treatment temperatures.

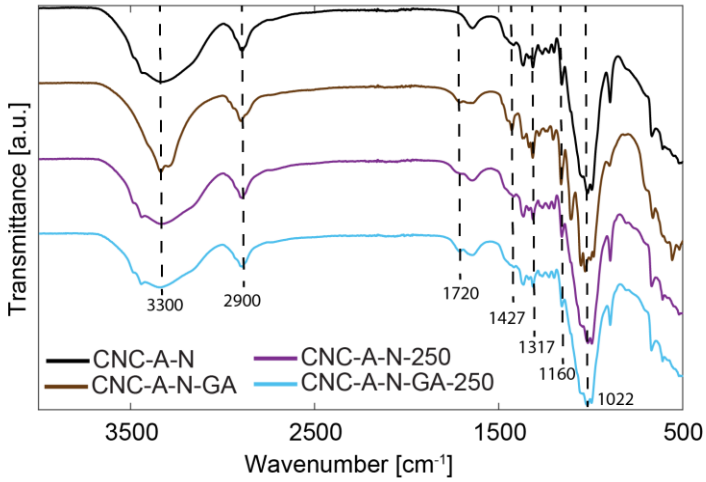

Figure 3. FTIR of CNC films before and after thermal treatment at 250 °C. FTIR measurement of CNC-A-N films and CNC-A-N-GA films before and after thermal treatment at 250 °C showing the typical cellulose transmittance peaks. Both the addition of cross-linker and the dehydration cause the observation of a C=O double bond (1720 cm^{-1}).

The chemical stability of cross-linked CNC-A-N-GA films at high temperatures was also quantified by thermogravimetric analysis (TGA) as reported in Figure 4. The thermal behaviour of the cross-linked films is compared to the films cast from an acidic suspension (CNC-A) and to films treated with KOH for 24 h (CNC-A-N). GA cross-linking induces a lower degradation onset temperature, T_{onset} = 260 °C, compared to the CNC film only treated with KOH, T_{onset} ~ 300 °C, as reported in Table S2; this can be caused by residual bound water in the CNC films, retained by the presence of unreacted GA, which provides additional oxygen to promote the cellulose degradation into volatile carbon species (Kim et al., 2001). However, GA crosslinking promotes a more gradual weight loss (occurring over a broader range of temperatures) than for CNC-A and CNC-A-N films. Interestingly, while the CNC-A is rapidly degrading between 150 °C and 200 °C compared to the CNC-A-N, its final residue is larger than the CNC-A-N above 300 °C, presumably due to the heat-induced release of free sulfuric acid (Kim et al., 2001). Comparatively, the CNC-A-N-GA allows for both a higher degradation

temperature than CNC-A and a similarly improved final residue of 26.8% for CNC-A-N-GA films *vs* 22.3% for CNC-A-N films. The CNC-A-N-GA option thus suggests overall improved chemical stability at lower temperature and increased final residue at higher temperature.

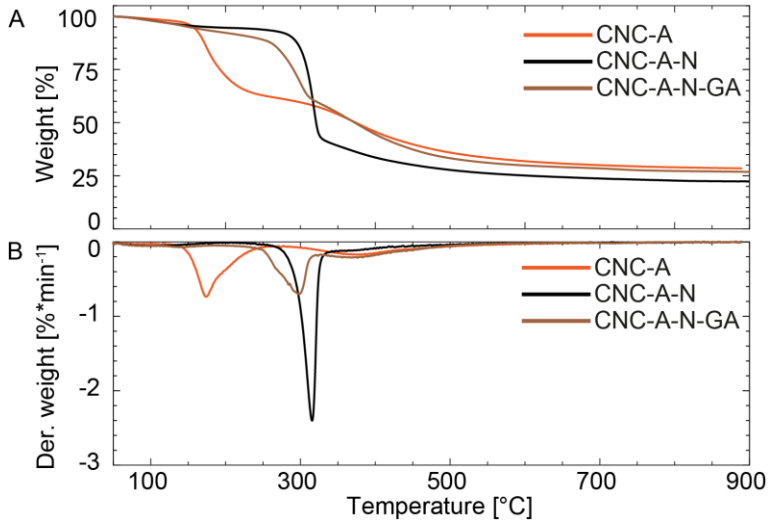

Figure 4. Thermogravimetric curves of CNC films. (**A**) Weight variation as a function of the thermal treatment temperature and (**B**) corresponding derivative curves for CNC-A films, CNC-A-N films, and for CNC-A-N-GA films.

Further increase of the temperature of thermal treatment of CNCs leads to the progressive decomposition of cellulose in an amorphous carbon structure, which may retain the initial helicoidal arrangement of the CNCs, depending on the applied thermal treatment (Dumanli & Windle, 2012; Titirici et al., 2015). However, the complete transformation of the crystalline cellulose in amorphous carbon is likely to cause the loss of the intrinsic birefringence that is characteristic of the anisotropic crystalline structure of cellulose, on top of increasing light absorption. Since the selective reflectance of circularly polarised light arises from the birefringent nature of the helicoidally arranged CNCs, fully carbonised CNC films that lost their birefringence are not expected to selectively reflect LCP light, regardless of whether the initial helicoidal arrangement is preserved. This is in contrast to opal structures, which can still retain their photonic response after high temperature thermal treatments (Gil-Herrera et al., 2018). The thermal treatment of CNC-A-N-GA films up to 900 °C presented, indeed, no

apparent polarization selectivity after cellulose decomposition into carbon and showed no sign of underlying helicoidal architecture (Figure S3).

Chiral nematic CNC films have previously been used as templates for the fabrication of chiral carbon for, *e.g.*, electrochemical and catalysis applications (Lizundia et al., 2017; Nguyen et al., 2019; Shopsowitz et al., 2011; Walters et al., 2020). One way to retain the helicoidal architecture for temperatures as high as 900 °C is to mix CNCs with a sol-gel precursor with high thermal stability. This enables the transformation of cellulose into carbon while also preserving the helicoidal arrangement (Shopsowitz et al., 2011). Here we show that sol-gel structural elements are actually not necessary to preserve the helicoidal architecture and that the direct fabrication of chiral carbon can be achieved by postprocessing optimisation of the surface charges of CNCs chiral nematic films. CNC films were cast in acidic conditions and desiccated at low-temperatures (CNC-A-Vac), allowing for the removal of water traces and the release of sulfate half ester groups (Bardet et al., 2015; Beck-Candanedo et al., 2005; Beck & Bouchard, 2014).

Before pyrolysis, the films displayed a helicoidal nanoarchitecture, as confirmed by the brilliant blue colouration (Figure S2), and by the strong reflectance peak at $\lambda \approx 450$ nm observed in LCP only, Figure 5, A and B (T_{room}), suggesting a pitch about $p \approx 290$ nm (assuming $n = 1.55$). Note that the cross-sectional images of the films in SEM (at low and intermediate resolutions) are consistent with this periodicity, but did not allow for a precise pitch comparison due to insufficient resolution (Figure S4).

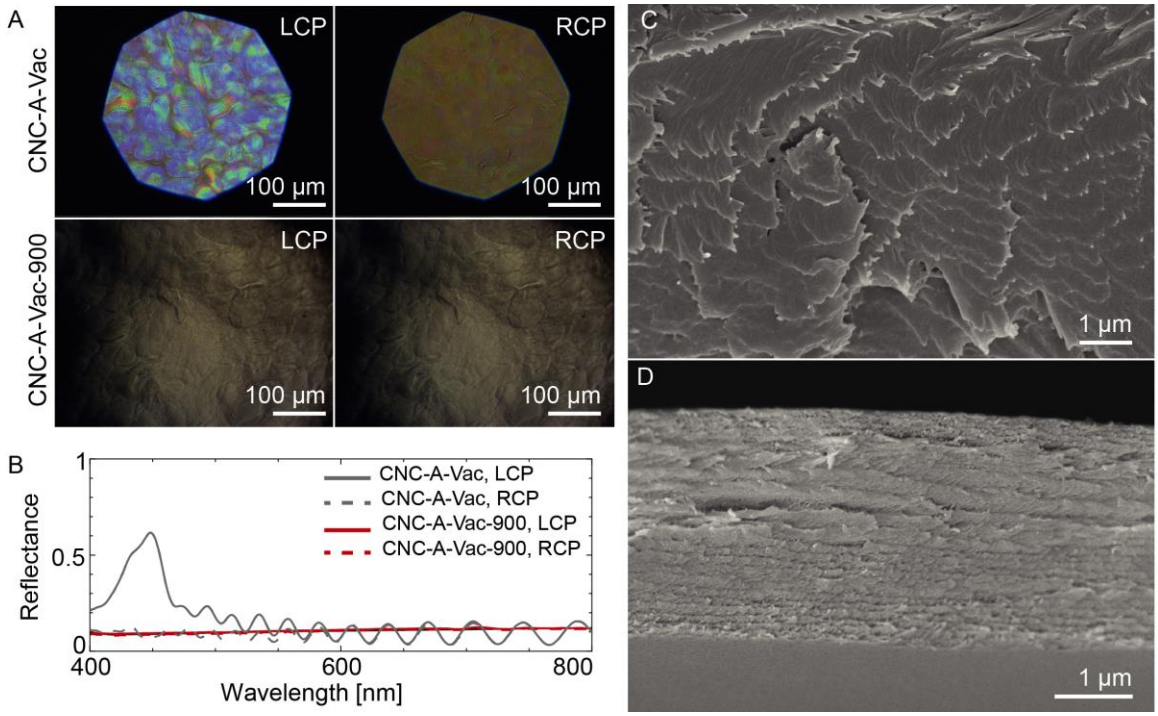

Figure 5. Polarised optical microscopy and SEM analysis of the vacuum-treated CNC films. (**A**) Polarised optical micrographs of CNC films before (CNC-A-Vac) and after (CNC-A-Vac-900) the pyrolysis in left- and right-circular polarisation channel, respectively LCP and RCP. (**B**) Corresponding reflectance spectra normalised with respect to a silver mirror in one polarisation channel. (**C**) High magnification SEM image of a delaminating area of the heat-treated films showing the arcing of the rods typical of chiral nematic films, and (**D**) cross-sections showing the pseudo-layer arrangement and the individual carbonaceous nanorods.

After the pyrolysis at 900 °C, the films appear colourless both in LCP and in RCP as shown in Figure 5A ($T_{900°C}$). No chiral difference in the reflectance signal of the films in LCP and RCP can be observed in the range 400–800 nm (Figure 5B), suggesting either the presence of a helicoidal architecture reflecting outside of the visible range (in this case in the UV due to the thermally-induced shrinkage of the sample), a strong absorbance given by the aromatic carbon (Figure S2), a loss of the birefringence of the helicoidal architecture, or the complete thermal degradation of the helicoidal arrangement. However, helicoidal architectures in CNC films were visible after the thermal treatment in SEM images (Figure 5C, D). The helicoidal arrangement is seen both in top view (Figure 5C) in delaminating areas of the films and in cross-sections (Figure 5D). These observations ruled out the thermal degradation of the helicoidal architecture as the main cause of the colour loss. Regardless of the birefringence loss that could have happened upon carbonisation, the pitch of the retained helicoidal architecture

is of the order of 215-235 nm, therefore too small to induce selective reflection above 400 nm to appear in the visible range (Parker et al., 2018). Interestingly, the shape of the original cellulose nanorods appeared to be retained in the carbonaceous structure, as well as heterogeneities in the pitch and in the cut; this indicates minimal thermal deformation of the cellulose nanocrystals shape during the thermal treatment, making it an interesting system for producing hierarchically organized 3D carbonaceous materials (Gil-Herrera et al., 2020; Herou et al., 2019; Kubo et al., 2013; Shopsowitz et al., 2011; Yan et al., 2016). While the helicoidal architecture of the films was retained for thermal treatments at 900 °C, this was not uniformly observed throughout the films' cross-section. This variation in the carbon nanoarchitecture possibly arises from CNC films heterogeneities in terms of defects presence and concentration of sulfuric acid in the dry film that can induce different carbonisation sequences. The CNC films heat treated at 900 °C appeared to be more brittle, which could be caused by a partial lack of interconnected hierarchical structure in the films. Despite requiring further investigation, the retained helicoidal arrangement is thought to be promoted by the low temperature desiccation process that allows to remove residual water traces as well as sulfate half ester groups that would, otherwise, promote a harsh cellulose degradation during the high temperature heat treatment. Finally, to further confirm the evolution of the cellulose structure in a carbonaceous material, FTIR measurements on the CNC-A-Vac samples before and after the thermal treatment at 900 °C were performed, see Figure S5. The typical cellulose transmittance peaks are clearly visible for CNC-A-Vac films before the pyrolysis but are mostly absent after the thermal treatment. The low intensity transmittance peaks at 3300, 2900 and 1022 cm^{-1} indicate the presence of, respectively, few residual O-H, C-H and C-O bonds in the carbonaceous material.

4. Conclusions

In this work, we have reported the effect of various heat treatments on the optical and structural properties of CNC films. First, we demonstrated that, by immersing chiral nematic CNC films in a concentrated base, cross-linking the KOH-treated CNC films with glutaraldehyde, and then thermally treating them in inert atmosphere, we can retain colour and selective LCP reflectance up to 250 °C. At this temperature, and due to the first signs of cellulose pyrolysis, the colour shown by the films is a combination of structural colour, caused by the cellulose chiral nematic assembly, and a yellowish pigmentation, attributed to the cellulose thermal degradation by-products, giving a golden shine to the resulting films. Cross-linking CNC films with GA allows for an improvement of the macroscopic colour appearance for intermediate thermal treatment temperatures (T=250 °C), minimizing the thermal darkening induced by the release of sulfuric acid. Therefore, this method can be used to adjust the optical response of chiral nematic CNC films by inducing a controlled darkening of the cellulose, useful in situations when the colouring end-use cannot rely on a dark background to enhance the structural colour component (*e.g.*, glitter dispersed in a fluid or on light skin), or when the simple addition of dark pigments (such as carbon black and melanin) might compromise the formation of a chiral nematic liquid crystalline phase in the first place. Similarly, the improved colour contrast of chiral nematic CNC films exposed at temperatures up to 250 °C makes them promising as passive colorimetric sensors of past heat exposure. Second, we showed that thermal treatments of chiral nematic CNC films at 900 °C lead to cellulose decomposition in amorphous carbon with helicoidal arrangement of the cellulose nanorods retained in some regions, thus producing chiral carbon. This latter ability is relevant for the fabrication of conductive carbon for electrodes with controlled morphology.

Author contributions:

Giulia Guidetti: Conceptualization, Methodology, Investigation, Data curation, Formal analysis, Validation, Visualization, Writing-original draft. **Bruno Frka-Petesic**: Conceptualization, Methodology, Investigation, Data curation, Formal analysis, Validation, Visualization, Supervision, Writing-original draft. **Wadood Y. Hamad**: Conceptualization, Resources, Formal analysis. **Ahu G. Dumanli**: Conceptualization, Methodology, Formal analysis, Supervision. **Silvia Vignolini**: Conceptualization, Funding acquisition, Resources, Methodology, Formal analysis, Visualization, Project administration, Supervision, Writing-original draft.

Acknowledgments

This work was supported by BBSRC [BB/K014617/1], EPSRC [1525292], EPRSC [EP/R511675/1], EPRSC [EP/K503757/1], European Research Council [ERC-2014-STG H2020 639088, ERC-PoC-2017 790518]. AGD would like to acknowledge the funding from bp for her bp-ICAM Kathleen Lonsdale Research Fellowship.

Declaration of interests: None.

Bibliography

Acierno, F. D. ', Hamad, W. Y., Michal, C. A., & Maclachlan, M. J. (2020). Thermal Degradation of Cellulose Filaments and Nanocrystals. *Biomacromolecules*. https://doi.org/10.1021/acs.biomac.0c00805

Bardet, R., Roussel, F., Coindeau, S., Belgacem, N., & Bras, J. (2015). Engineered pigments based on iridescent cellulose nanocrystal films. *Carbohydrate Polymers*, *122*, 367–375. https://doi.org/10.1016/j.carbpol.2014.10.020

Beck-Candanedo, S., Roman, M., & Gray, D. G. (2005). Effect of reaction conditions on the properties and behavior of wood cellulose nanocrystal suspensions. *Biomacromolecules*, *6*(2), 1048–1054. https://doi.org/10.1021/bm049300p

Beck, S., & Bouchard, J. (2014). Auto-catalyzed acidic desulfation of cellulose nanocrystals. *Nordic Pulp and Paper Research Journal*, *29*(1), 6–14. https://doi.org/10.3183/npprj-2014-29-01-p006-014

Beck, S., Bouchard, J., Chauve, G., & Berry, R. (2013). Controlled production of patterns in iridescent solid films of cellulose nanocrystals. *Cellulose*, *20*(3), 1401–1411. https://doi.org/10.1007/s10570-013-9888-4

Brown, E. E., Laborie, M. P. G., & Zhang, J. (2012). Glutaraldehyde treatment of bacterial cellulose/fibrin composites: Impact on morphology, tensile and viscoelastic properties. *Cellulose*, *19*(1), 127–137. https://doi.org/10.1007/s10570-011-9617-9

Camarero Espinosa, S., Kuhnt, T., Foster, E. J., & Weder, C. (2013). Isolation of thermally stable cellulose nanocrystals by phosphoric acid hydrolysis. *Biomacromolecules*, *14*(4), 1223–1230. https://doi.org/10.1021/bm400219u

Cao, Y., Wang, P., D'Acierno, F., Hamad, W. Y., Michal, C. A., & MacLachlan, M. J. (2020). Tunable Diffraction Gratings from Biosourced Lyotropic Liquid Crystals. *Advanced Materials*, *32*(19), 1907376. https://doi.org/10.1002/adma.201907376

Chan, C. L. C., Bay, M. M., Jacucci, G., Vadrucci, R., Williams, C. A., van de Kerkhof, G. T., Parker, R. M., Vynck, K., Frka-Petesic, B., & Vignolini, S. (2019). Visual Appearance of Chiral Nematic Cellulose-Based Photonic Films: Angular and Polarization Independent Color Response with a Twist. *Advanced Materials*, *31*(52), 1905151. https://doi.org/10.1002/adma.201905151

Dai, W. S., & Barbari, T. A. (1999). Hydrogel membranes with mesh size asymmetry based on the gradient crosslinking of poly (vinyl alcohol). *Journal of Membrane Science*, *156*(1 LB-dai1999), 67–79.

Dong, X. M., Revol, J.-F., & Gray, D. G. (1998). Effect of microcrystallite preparation conditions on the formation of colloid crystals of cellulose. *Cellulose*, *5*(1), 19–32. https://doi.org/10.1023/A:1009260511939

Dumanli, A. G., van der Kooij, H. M., Kamita, G., Reisner, E., Baumberg, J. J., Steiner, U., & Vignolini, S. (2014). Digital Color in Cellulose Nanocrystal Films. *ACS Applied Materials & Interfaces*, *6*(15), 12302–12306. https://doi.org/10.1021/am501995e

Dumanli, A. G., & Windle, A. H. (2012). Carbon fibres from cellulosic precursors: A review. In *Journal of Materials Science* (Vol. 47, Issue 10, pp. 4236–4250). https://doi.org/10.1007/s10853-011-6081-8

Elazzouzi-Hafraoui, S., Nishiyama, Y., Putaux, J. L., Heux, L., Dubreuil, F., & Rochas, C. (2008). The shape and size distribution of crystalline nanoparticles prepared by acid hydrolysis of native cellulose. *Biomacromolecules*, *9*(1), 57–65. https://doi.org/10.1021/bm700769p

Eyley, S., & Thielemans, W. (2014). Surface modification of cellulose nanocrystals. *Nanoscale*, *6*(14), 7764–7779. https://doi.org/10.1039/c4nr01756k

Frka-Petesic, B., Guidetti, G., Kamita, G., & Vignolini, S. (2017). Controlling the Photonic

509 Properties of Cholesteric Cellulose Nanocrystal Films with Magnets. *Advanced*
510 *Materials*, *29*(32), 1–7. https://doi.org/10.1002/adma.201701469
511 Frka-Petesic, B., Kamita, G., Guidetti, G., & Vignolini, S. (2019). Angular optical response
512 of cellulose nanocrystal films explained by the distortion of the arrested suspension
513 upon drying. *Physical Review Materials*, *3*(4).
514 https://doi.org/10.1103/PhysRevMaterials.3.045601
515 Frka-Petesic, B., Radavidson, H., Jean, B., & Heux, L. (2017). Dynamically Controlled
516 Iridescence of Cholesteric Cellulose Nanocrystal Suspensions Using Electric Fields.
517 *Advanced Materials*, *29*(11), 1606208. https://doi.org/10.1002/adma.201606208
518 Frka-Petesic, B., Sugiyama, J., Kimura, S., Chanzy, H., & Maret, G. (2015). Negative
519 Diamagnetic Anisotropy and Birefringence of Cellulose Nanocrystals. *Macromolecules*,
520 *48*(24), 8844–8857. https://doi.org/10.1021/acs.macromol.5b02201
521 Gil-Herrera, L. K., Gallego-Gómez, F., Torres-Pardo, A., González-Calbet, J. M., Palomares,
522 F. J., Blanco, A., Juárez, B. H., & López, C. (2020). Silicon-Based Photonic
523 Architectures from Hierarchically Porous Carbon Opals. *Particle and Particle Systems*
524 *Characterization*, *37*(1), 1900396. https://doi.org/10.1002/ppsc.201900396
525 Gil-Herrera, L. K., Pariente, J. A., Gallego-Gómez, F., Gándara, F., Juárez, B. H., Blanco, Á.,
526 & López, C. (2018). Hierarchically Porous Carbon Photonic Structures. *Advanced*
527 *Functional Materials*, *28*(27), 1703885. https://doi.org/10.1002/adfm.201703885
528 Guidetti, G., Atifi, S., Vignolini, S., & Hamad, W. Y. (2016). Flexible Photonic Cellulose
529 Nanocrystal Films. *Advanced Materials*, *28*(45), 10042–10047.
530 https://doi.org/10.1002/adma.201603386
531 Hamad, W. Y., & Hu, T. Q. (2010). Structure-process-yield interrelations in nanocrystalline
532 cellulose extraction. *Canadian Journal of Chemical Engineering*, *88*(3), 392–402.
533 https://doi.org/10.1002/cjce.20298
534 Hennink, W. E., & van Nostrum, C. F. (2012). Novel crosslinking methods to design
535 hydrogels. *Advanced Drug Delivery Reviews*, *64*(SUPPL.), 223–236.
536 https://doi.org/10.1016/j.addr.2012.09.009
537 Herou, S., Ribadeneyra, M. C., Madhu, R., Araullo-Peters, V., Jensen, A., Schlee, P., &
538 Titirici, M. (2019). Ordered mesoporous carbons from lignin: a new class of biobased
539 electrodes for supercapacitors. *Green Chemistry*, *21*(3), 550–559.
540 https://doi.org/10.1039/C8GC03497D
541 Kim, D. Y., Nishiyama, Y., Wada, M., & Kuga, S. (2001). High-yield carbonization of
542 cellulose by sulfuric acid impregnation. *Cellulose*, *8*(1), 29–33.
543 https://doi.org/10.1023/A:1016621103245
544 Kubo, S., White, R. J., Tauer, K., & Titirici, M.-M. (2013). *Flexible Coral-like Carbon*
545 *Nanoarchitectures via a Dual Block Copolymer−Latex Templating Approach*.
546 https://doi.org/10.1021/cm4029676
547 Lazko, J., Sénéchal, T., Landercy, N., Dangreau, L., Raquez, J. M., & Dubois, P. (2014).
548 Well defined thermostable cellulose nanocrystals via two-step ionic liquid swelling-
549 hydrolysis extraction. *Cellulose*, *21*(6), 4195–4207. https://doi.org/10.1007/s10570-014-
550 0417-x
551 Lin, N., & Dufresne, A. (2014). Surface chemistry, morphological analysis and properties of
552 cellulose nanocrystals with gradiented sulfation degrees. *Nanoscale*, *6*(10), 5384–5393.
553 https://doi.org/10.1039/c3nr06761k
554 Lizundia, E., Nguyen, T. D., Vilas, J. L., Hamad, W. Y., & MacLachlan, M. J. (2017).
555 Chiroptical, morphological and conducting properties of chiral nematic mesoporous
556 cellulose/polypyrrole composite films. *Journal of Materials Chemistry A*, *5*(36), 19184–
557 19194. https://doi.org/10.1039/c7ta05684b
558 Mane, S., Ponrathnam, S., & Chavan, N. (2016). Effect of Chemical Crosslinking on

559 Properties of Polymer Microbeads: A Review. *Canadian Chemical Transactions*, *3*(4),
560 473–485. https://doi.org/10.13179/canchemtrans.2015.03.04.0245
561 Marchessault, R. H., Morehead, F. F., & Walter, N. M. (1959). Liquid Crystals Systems from
562 Fibrillar Polysaccharides. *Nature*, *184*(4686), 632–633.
563 https://doi.org/10.1038/184632a0
564 Migneault, I., Dartiguenave, C., Bertrand, M. J., & Waldron, K. C. (2004). Glutaraldehyde:
565 Behavior in aqueous solution, reaction with proteins, and application to enzyme
566 crosslinking. In *BioTechniques* (Vol. 37, Issue 5, pp. 790–802). Eaton Publishing
567 Company. https://doi.org/10.2144/04375rv01
568 Nan, F., Nagarajan, S., Chen, Y., Liu, P., Duan, Y., Men, Y., & Zhang, J. (2017). Enhanced
569 Toughness and Thermal Stability of Cellulose Nanocrystal Iridescent Films by Alkali
570 Treatment. *ACS Sustainable Chemistry and Engineering*, *5*(10), 8951–8958.
571 https://doi.org/10.1021/acssuschemeng.7b01749
572 Nguyen, T., Li, J., Lizundia, E., Niederberger, M., Hamad, W. Y., & MacLachlan, M. J.
573 (2019). Black Titania with Nanoscale Helicity. *Advanced Functional Materials*, *29*(40),
574 1904639. https://doi.org/10.1002/adfm.201904639
575 Parker, R. M., Frka-petesic, B., Guidetti, G., Kamita, G., Consani, G., Abell, C., & Vignolini,
576 S. (2016). Hierarchical Self-Assembly of Cellulose Nanocrystals in a Confined
577 Geometry. *ACS Nano*, *10*(9), 8443–8449. https://doi.org/10.1021/acsnano.6b03355
578 Parker, R. M., Guidetti, G., Williams, C. A., Zhao, T., Narkevicius, A., Vignolini, S., & Frka-
579 Petesic, B. (2018). The Self-Assembly of Cellulose Nanocrystals: Hierarchical Design
580 of Visual Appearance. *Advanced Materials*, *30*(19), 1–13.
581 https://doi.org/10.1002/adma.201704477
582 Revol, J.-F. F., Bradford, H., Giasson, J., Marchessault, R. H., & Gray, D. G. (1992).
583 Helicoidal self-ordering of cellulose microfibrils in aqueous suspension. *International*
584 *Journal of Biological Macromolecules*, *14*(3), 170–172. https://doi.org/10.1016/S0141-
585 8130(05)80008-X
586 Revol, J.-F. F., Godbout, L., & Gray, D. G. (1998). Solid self-assembled films of cellulose
587 with chiral nematic order and optically variable properties. *Journal of Pulp and Paper*
588 *Science*, *24*(5), 146–149.
589 Revol, J.-F., Godbout, D. L., & Gray, D. G. (1997). Solidified liquid crystals of cellulose
590 with optically variable properties. *US Patent 5,629,055*, *28*(14 LB-revol1997p), 9.
591 Revol, J., & Goring, D. A. I. (1981). On the mechanism of the mercerization of cellulose in
592 wood. *Journal of Applied Polymer Science*, *26*(4 LB-revol1981), 1275–1282.
593 Roman, M., & Winter, W. T. (2004). Effect of sulphate groups from sulphuric acid
594 hydrolysis on the thermal degradation behaviour of bacterial cellulose.
595 *Biomacromolecules*, *5*, 1671–1677. https://doi.org/10.1021/BM034519+
596 Shopsowitz, K. E., Hamad, W. Y., & MacLachlan, M. J. (2011). Chiral nematic mesoporous
597 carbon derived from nanocrystalline cellulose. *Angewandte Chemie - International*
598 *Edition*, *50*(46), 10991–10995.
599 Titirici, M. M., White, R. J., Brun, N., Budarin, V. L., Su, D. S., Del Monte, F., Clark, J. H.,
600 & MacLachlan, M. J. (2015). Sustainable carbon materials. *Chemical Society Reviews*,
601 *44*(1), 250–290. https://doi.org/10.1039/c4cs00232f
602 Ţucureanu, V., Matei, A., & Avram, A. M. (2016). FTIR Spectroscopy for Carbon Family
603 Study. In *Critical Reviews in Analytical Chemistry* (Vol. 46, Issue 6, pp. 502–520).
604 https://doi.org/10.1080/10408347.2016.1157013
605 Vignolini, S., Gregory, T., Kolle, M., Lethbridge, A., Moyroud, E., Steiner, U., Glover, B. J.,
606 Vukusic, P., & Rudall, P. J. (2016). Structural colour from helicoidal cell-wall
607 architecture in fruits of Margaritaria nobilis. *Journal of the Royal Society Interface*,
608 *13*(124), 20160645. https://doi.org/10.1098/rsif.2016.0645

Walters, C. M., Adair, K. R., Hamad, W. Y., & MacLachlan, M. J. (2020). Synthesis of Chiral Nematic Mesoporous Metal and Metal Oxide Nanocomposites and their Use as Heterogeneous Catalysts. *European Journal of Inorganic Chemistry*, *2020*(41), 3937–3943. https://doi.org/10.1002/ejic.202000673

Wang, N., Ding, E., & Cheng, R. (2007). Thermal degradation behaviors of spherical cellulose nanocrystals with sulfate groups. *Polymer*, *48*(12), 3486–3493.

Wine, Y., Cohen-Hadar, N., Freeman, A., & Frolow, F. (2007). Elucidation of the mechanism and end products of glutaraldehyde crosslinking reaction by X-ray structure analysis. *Biotechnology and Bioengineering*, *98*(3), 711–718. https://doi.org/10.1002/bit.21459

Yan, B., Matsushita, S., & Akagi, K. (2016). An Advanced Method for Preparation of Helical Carbon and Graphitic Films Using a Carbonization Substrate. *Chemistry of Materials*, *28*(23), 8781–8791. https://doi.org/10.1021/acs.chemmater.6b04355

Zhao, T. H., Parker, R. M., Williams, C. A., Lim, K. T. P., Frka-Petesic, B., & Vignolini, S. (2019). Printing of Responsive Photonic Cellulose Nanocrystal Microfilm Arrays. *Advanced Functional Materials*, *29*(21), 1804531. https://doi.org/10.1002/adfm.201804531